We present the joint research of the Fraunhofer Institute for Ceramic Technologies and Systems IKTS and the Federal Institute for Materials Research and Testing BAM in Berlin.

Investigations on electron beam irradiated rare-earth doped SrF_2 for application as low fading dosimeter material: evidence for and DFT simulation of a radiation-induced phase

A synthesis of rare-earth doped SrF_2 nano powders, which are suitable as attractive low-fading dosimeter materials for electron irradiation. The low fading could be explained by secondary phase formation.

**ROYAL SOCIETY
OF CHEMISTRY**

rsc.li/materials-c

Registered charity number: 207890

PAPER

Check for updates

Investigations on electron beam irradiated rare-earth doped SrF$_2$ for application as low fading dosimeter material: evidence for and DFT simulation of a radiation-induced phase†

Michael Arnold, [ID] *[a] Julia Katzmann,[b] Aakash Naik, [ID] [cd] Arno L. Görne, [ID] [a] Thomas Härtling,[be] Janine George [ID] [cd] and Christiane Schuster[b]

A recent approach to measure electron radiation doses in the kGy range is the use of phosphors with an irradiation dose-dependent luminescence decay time. However, the applicability of the previously investigated material NaYF$_4$:Yb^{3+},Er^{3+} is limited as it shows pronounced fading. Therefore, in this work, a modified SrF$_2$ synthesis is presented that results in SrF$_2$ nanoparticles codoped with Yb and either Er, Hm, or Tm. To assess their suitability as dosimeter material, dose response, as well as its degree of fading over 50 up to 140 days after irradiation were measured. Fading rates as small as 5% in SrF$_2$:Er,Yb and 4% in SrF$_2$:Ho,Yb were derived, which are comparable to established dosimeter materials. A combination of spectroscopy, diffraction and DFT calculations was used to elucidate the effect of irradiation, pointing towards the formation of a secondary phase of Yb^{2+} that we predict could be Yb$_2$OF$_2$. This irreversible formation of a secondary phase is considered to be the explanation for the low fading behavior in SrF$_2$-based phosphors compared to NaYF$_4$:Yb, Er, a highly attractive feature for electron beam dosimetry.

Introduction

Electron beam (e-ebeam) irradiation is nowadays routinely used for food decontamination and other applications like radiation sterilization and enhancement of materials properties as it shows less effect on the quality of the treated products than competing methods.[1] Lately, low-energy electron beam treatments to limit the effects to the surface of the products have come into focus,[2] and have also been considered for vaccine manufacturing by inactivating pathogens.[3] However, because of their shape and thickness, currently available dosimeters based on optical or electron paramagnetic resonance read-out are not fully suited for usage in low energy e-beams and thus,

new materials are needed. Some inorganic phosphors are sensitive to ionizing radiation in a way that their luminescence decay time decreases as a result of the irradiation. It was first discovered almost 50 years ago in the phosphor barium ytterbium fluoride BaYb$_2$F$_8$:Er.[4–6] The transfer of this effect to the upconversion phosphor sodium yttrium fluoride NaYF$_4$:Er,Yb and the investigation of this material as a potential dosimetric material is, however, relatively new.[7,8] Although the precise nature of the radiation-induced effect in NaYF$_4$:Yb^{3+},Er^{3+} remains to be clarified, the decrease in luminescence decay time is attributed to a higher probability for non-radiative decay of the $^2F_{5/2}$ level in Yb^{3+}, in analogy to BaYb$_2$F$_8$:Er.[5] Nevertheless, the decay time of the luminescence is independent of its intensity, and, in case the phosphor is used as a dose-sensitive component for dosimetry, the measurement signal, in general, is not dependent on the dosimetric layer thickness or the amount of dosimetry material. This property is beneficial for low-energy e–e-beam dosimetry as, for example, it enables the application of thin dosimetric layers directly onto product surfaces to estimate the surface dose or to measure dose distributions on 3D surfaces.[9] However, the strong fading of the dose response hampers the application of NaYF$_4$:Er,Yb as a dosimeter material so far: the luminescence decay time re-increases partially over time after irradiation. Fading occurs so far to all radiation-sensitive materials and is extensively studied, for example, in

[a] Fraunhofer Institute for Ceramic Technologies and Systems (IKTS), Michael-Faraday-Strasse 1, 07629 Hermsdorf, Germany. E-mail: michael.arnold@ikts.fraunhofer.de

[b] Fraunhofer Institute for Ceramic Technologies and Systems (IKTS), Maria-Reiche-Strasse 2, 01109 Dresden, Germany

[c] Bundesanstalt für Materialforschung-und Prüfung, Unter den Eichen 87, 12205 Berlin, Germany

[d] Friedrich-Schiller-University Jena, Institute of Condensed Matter Theory and Solid State Optics, Max-Wien-Platz 1, 07743 Jena, Germany

[e] Institute for Solid State Electronics, Technische Universität Dresden, 01062 Dresden, Germany

† Electronic supplementary information (ESI) available. See DOI: **https://doi.org/10.1039/d2tc01773c**

This journal is © The Royal Society of Chemistry 2022

J. Mater. Chem. C, 2022, **10**, 11579–11587 | **11579**

thermoluminescence materials like calcium fluoride CaF_2:RE^{3+} [10] (RE stands for a rare earth element). To improve the applicability of decay time dosimetry, we searched for alternative dose-sensitive phosphors which are subject to less fading than $NaYF_4$:Er,Yb.

Therefore, in this work SrF_2:Er,Yb phosphor powders were synthesized, characterized, and the influence of electron radiation on their decay time was studied, as well as the associated fading of the reduced decay time. They are compared to $NaYF_4$:Er,Yb; also, two more dopants are tested in SrF_2:Ho,Yb and SrF_2:Tm,Yb. We identified a radiation-induced secondary phase formation in doped SrF_2:Er,Yb and a change in the fluorescence emission spectra. DFT calculations were employed to predict a stable structure for the secondary phase, and to form a hypothesis on the reason of the low decay time fading behavior of SrF_2:Er,Yb. The DFT-based data-driven structural prediction method utilized in this paper has previously been used successfully to forecast crystal structures of phosphors, among many other materials classes. [11,12] This approach uses data-mined ionic substitutions to predict new structures: such data-driven approaches are computationally significantly cheaper than exhaustive searches based on global optimization techniques in combination with DFT. [13]

Results and discussion

SrF_2 doped with erbium and ytterbium

Powder samples of sub-micron particles (100 nm size) were prepared by precipitation from aqueous solution, as described in the Experimental section. Fig. 1(a) shows X-ray diffractometry (XRD) data from SrF_2 doped with 2 mol% erbium and 2 to 20 mol% ytterbium. All reflections correspond to single phase powders of a fluorite type crystal structure in (JCPDS card 06-02612) and in the literature. [14,15] The measured reflections are compared to a PowderCell-simulation using the cell parameter [9] a = 5.799 Å for 2 mol% Yb^{3+} and 5.732 Å for 20 mol% Yb^{3+} (not shown).

The calculation of the cell parameters is presented in Fig. 1(b): in agreement with literature data, [10] a linear decrease of the cell parameter with increasing Yb^{3+} concentration is observed, which can be attributed to the smaller ion radius of the rare earth ions replacing the divalent Strontium in the unit cell. The phase diagram [17] of SrF_2–YbF_3 shows that a single phase solid solution exists up to 25% YbF_3. Upon the excitation with a 980 nm laser beam, the SrF_2:Yb^{3+},Er^{3+} material exhibits the typical narrow lines from Er^{3+} upconversion. Fig. 2(a) shows the typical emissions in the range of 537 and 544 nm, which are ascribed to the $^2H_{11/2} \rightarrow {}^4I_{15/2}$ and $^4S_{3/2} \rightarrow {}^4I_{15/2}$ transitions, [18] and also an emission at 655 nm. With increasing ytterbium concentration, the intensity of the 655 nm emission, originating from the $^4F_{9/2} \rightarrow {}^4I_{15/2}$ transition, also increases. This occurs because the energy transfer upconversion (ETU) process from $^2H_{11/2}$ to ^4G, ^2K is enhanced with higher ytterbium content [19] (Fig. 2(b)). The decay times are always lower for the considered upconversion emissions than for those from positive Stokes shifts (as are the emission intensities), and we find the same when comparing our co-doped samples to only Yb^{3+}-doped
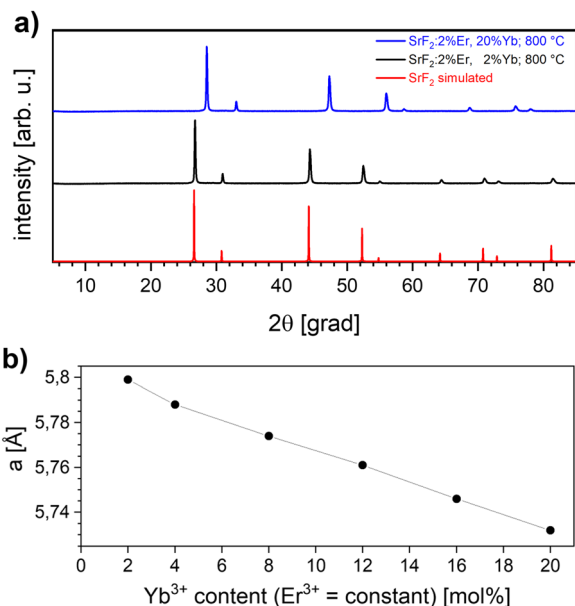

Fig. 1 (a) Representative X-ray diffractograms of SrF_2: 2 mol% Er^{3+}, 2 mol% Yb^{3+} (black line) and SrF_2: 2 mol% Er^{3+}, 20 mol% Yb^{3+} sample (blue line) calcined at 800 °C and TOPAZ-simulation of SrF_2 (red line). (b) The calculated cell parameter from XRD-data for calcined SrF_2: 2 mol% Er^{3+}, x mol% Yb^{3+} for x = 2–20 (line guide to the eye).
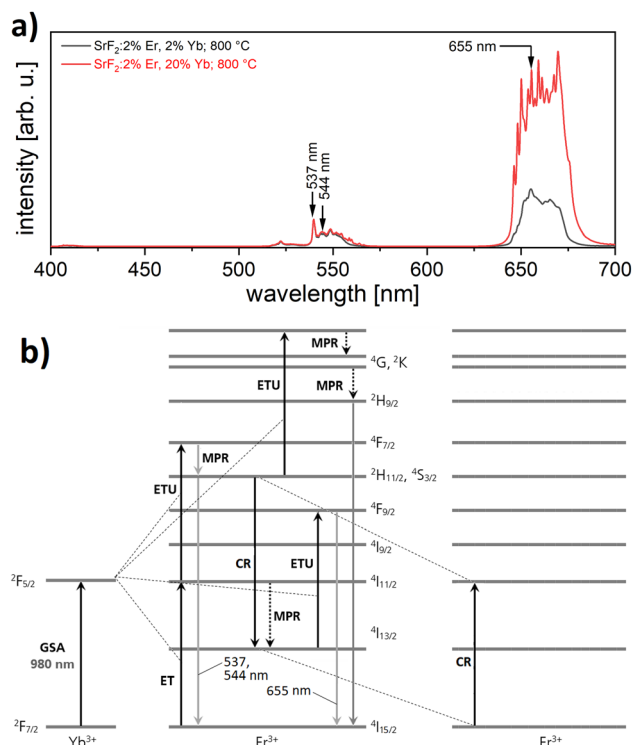

Fig. 2 (a) Luminescence spectra of SrF_2:Er,Yb powder (visible range) upon excitation with 980 nm laser light. The spectra are normalized to the peak at 540 nm. (b) Model of the well-known UC process in SrF_2:Er^{3+},Yb^{3+} (adopted from Lyapin et al. [18]). GSA: ground state absorption, MPR: multiphonon relaxation, CR: cross relaxation.

11580 | *J. Mater. Chem. C*, 2022, **10**, 11579–11587

This journal is © The Royal Society of Chemistry 2022

SrF_2.[20] Between 2 and 20 at% doping with trivalent ytterbium, a decrease in the decay time of 400 µs oat the upconversion emission was observed (not shown here). A similar decrease of the decay time with the increase of the Yb^{3+} concentration was described for the case of Yb^{3+} fluorescence.[20] The emission intensity at 544 nm is most intense with 2 at% erbium co-doping, while concentrations of 1, 2, 3, and 5 at% were investigated.

Fig. 3(a) and (b) show the field emission scanning electron microscopy (FE-SEM) images of the material, as precipitated and calcined at 800 °C, respectively. Agglomerated particles of approximately 100 nm size can be seen. Particle size decreases slightly after calcination and XRD reflections become sharper (data not shown) as a result of improved crystallinity and a decrease of microstrains.[16] Annealing temperatures of 600, 700, and 800 °C were used for our powders, giving almost identical emission intensities. Higher temperatures than that already led to degradation of SrF_2 in air. This agrees very well with the observations of the thermoluminescence on ceramic pellets in the literature.[21]

After electron beam irradiation (200 keV) of a thin immobilized phosphor layer, the luminescence decay time of the SrF_2: 2%Er, 2%Yb phosphor decreases from 1520 µs to values between 1250 and 1020 µs, depending on the irradiation dose, as shown in Fig. 4(a). For doses up to 10 kGy, a strong dose dependence is evident that becomes weaker as the irradiation increases further and seems to saturate above 50 kGy. The initial (*i.e.* measured within minutes after irradiation) decay time reduction for 50 kGy amounts to 30%. Comparing these results with the dose response of $NaYF_4$:Er,Yb (purchased from Honeywell; refer to Reitzig *et al.*[8] for the dose reponse curve), we see the following: (1) the shapes of the dose response curves are comparable. (2) $NaYF_4$:Er,Yb shows a greater initial decrease of its decay time upon radiation (90% for 50 kGy).

For SrF_2:Er,Yb samples irradiated with 5, 10 and 20 kGy, the luminescence decay times were repeatedly measured until 50 days after irradiation (Fig. 4(b) and (c)). They increased in the first day of storage at 20 °C (first and second measurements) towards the initial value, but, during the following two days, the decay times remained almost constant. Looking into the decay

times 25 to 50 days after irradiation (Fig. 4(b)), they only slightly increased compared to day 2 and 3. Furthermore, between the 25th and 50th day, the decay time did not rise anymore, and the fading therefore appeared to have finished. On the other hand, we can see that the decay time of $NaYF_4$:Er,Yb rose strongly in the first days after irradiation (Fig. 4(d)). It still rose between the 25th and 50th day, although slower and to values much lower than the unirradiated sample (650–800 µs *vs.* 1220 µs initially).

Clearly, one day after irradiation, the decay time of SrF_2:Er,Yb was already close to the long-term value and could be read out in a dosimeter with sufficient precision. In fact, after 50 days of storage, the decay time of SrF_2:Er,Yb had increased by only 5% with respect to the first measurement after irradiation. This degree of fading is comparable to established dosimeter materials, *e.g.* 2–5% in alanine over 100 days after 14 kGy irradiation.[22] For a possible application as an electron radiation dosimetry material, this very low fading of SrF_2:Er,Yb outweighs the lower dose resolution compared to $NaYF_4$:Er,Yb.

SrF₂ doped with holmium/ytterbium and thulium/ytterbium

To build on these results, $Sr_{1-x-y}Ho_xYb_yF_2$ and $Sr_{1-x-y}Tm_x Yb_yF_2$ powders were synthesized in the same way as SrF_2:Er,Yb. The effect of very low fading could also be observed in Ho/Yb and Tm/Yb codoping.

The optimum concentration of the dopants Yb and Ho or Tm for highest upconversion emission intensity (Fig. 5) was determined for $x = 0.02$, $y = 0.2$ (for Ho and Yb) and $x = 0.01$, $y = 0.2$ (for Tm and Yb). All subsequent measurements were carried out with these doping concentrations. The powders were calcined at 600 °C. Fig. 6(a) and (b) show the X-ray diffractograms of the samples $Sr_{0.78}Ho_{0.02}Yb_{0.2}F_2$ and $Sr_{0.79}Tm_{0.01}Yb_{0.2}F_2$ in comparison with the simulated SrF_2 diffractogram. Despite the high contents of trivalent rare earth ions, no secondary phases could be observed. This corresponds well to the literature[18,23] in which no phase changes were observed for RE doping concentrations up to 20 mol% for the calcination temperature of 600 °C used here.

The dependence of the cell parameter on the Yb content for codoped SrF_2 is shown in Table 1. A shift to higher diffraction
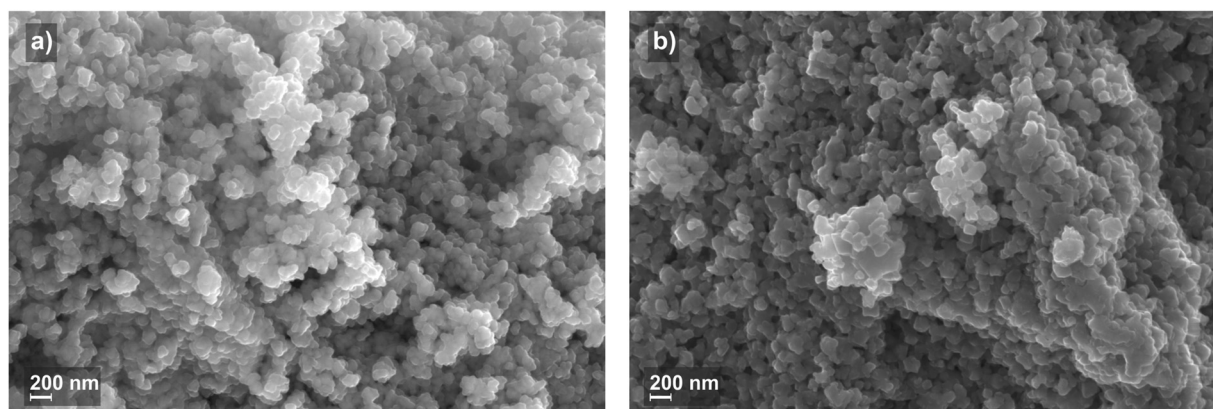

Fig. 3 FE-SEM micrographs of SrF_2: 2 mol% Er^{3+}, 2 mol% Yb^{3+}. (a) The precipitated material and (b) the at 800 °C calcined material.

This journal is © The Royal Society of Chemistry 2022

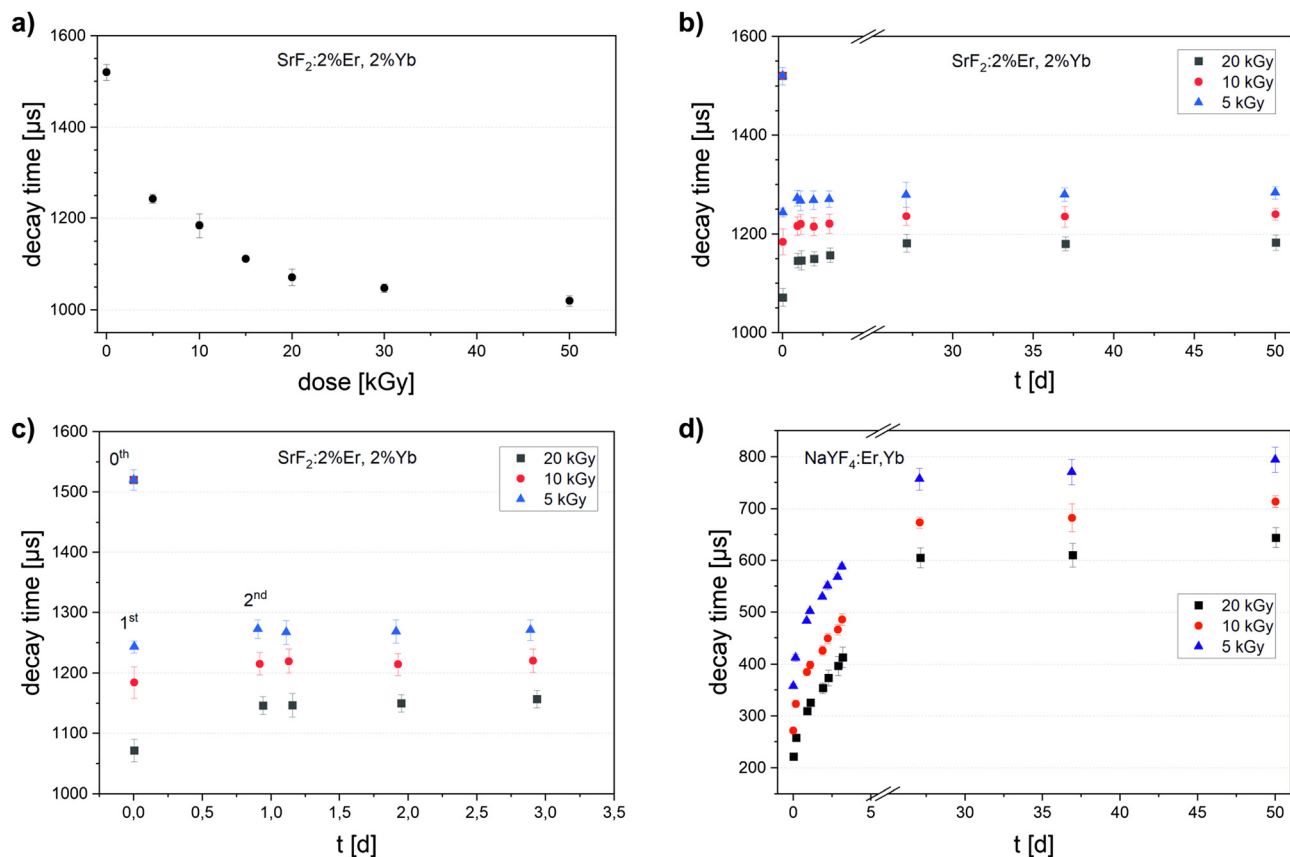*J. Mater. Chem. C*, 2022, **10**, 11579–11587 | **11581**

Fig. 4 (a) Luminescence decay times of SrF$_2$: 2 mol% Er^{3+}, 2 mol% Yb^{3+} after 200 keV electron irradiation with the given doses (dose response curve). (b) Luminescence decay times of SrF$_2$: 2 mol% Er^{3+}, 2 mol% Yb^{3+} irradiated with 5, 10 and 20 kGy up to 50 days after irradiation (fading curve). (c) The same fading curve as before, shown only for the first three days (0th measurement represents decay times before irradiation). (d) Fading curve of NaYF$_4$:Er,Yb up to 50 days after irradiation for comparison; decay time before irradiation is 1224 µs ± 8 µs (not shown in the diagram).
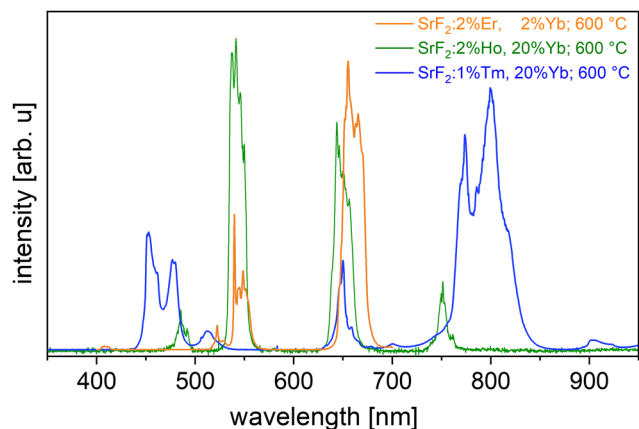

Fig. 5 UC emission of Yb doped SrF$_2$ codoped with Er (orange line), Holmium (green line) and Thulium (blue line).
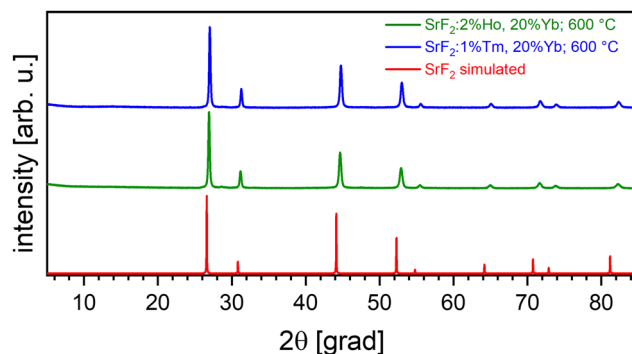

Fig. 6 X-ray diffractograms of Yb-doped Strontium fluoride codoped with Ho (green) and Tm (blue).

angles is observable (Fig. 6) with respect to the simulated SrF$_2$ diffractogram.

After electron beam irradiation (200 keV) of a thin immobilized phosphor layer, the luminescence decay time of the SrF$_2$:Ho,Yb and SrF$_2$:Tm,Yb phosphors decrease from 95 and

Table 1 Change of the cell parameter a with Yb doping level and different codopants

Codoping	None	Er (2 mol%)		Ho (2 mol%)		Tm (1 mol%)	
Yb (at %)	None	2	20	2	20	1	20
a (Å)	5.799	5.789(4)	5.736(4)	5.782(2)	5.737(6)	5.782(4)	5.738(3)

11582 | *J. Mater. Chem. C*, 2022, **10**, 11579–11587

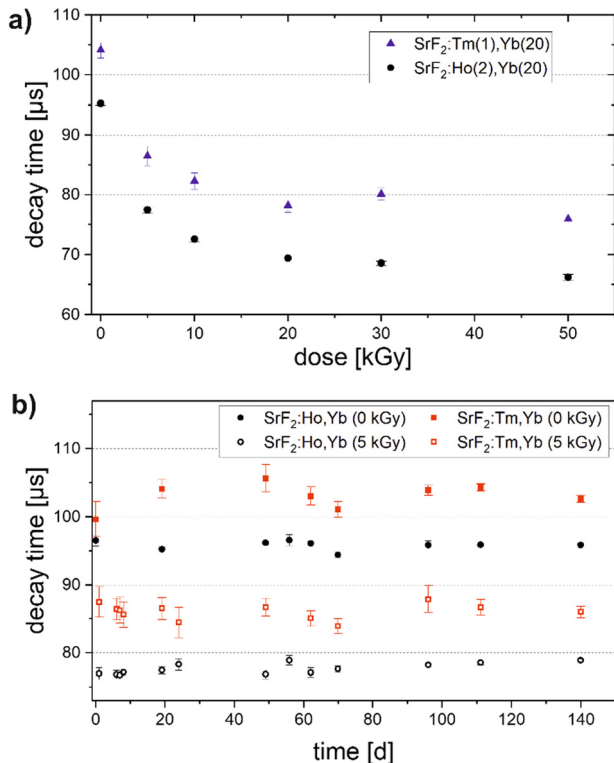This journal is © The Royal Society of Chemistry 2022

Fig. 7 (a) Dose response of the decay time of thin layers of SrF_2 powder codoped with Tm, Yb or Ho, Yb upon 200 keV electron radiation. (b) Luminescence decay times of SrF_2:Tm,Yb and SrF_2:Ho,Yb phosphor samples (unirradiated and irradiated with 5 kGy) over the course of 140 days starting from day 1 after irradiation.

104 µs, respectively, to values which are 15 to 30 µs lower, depending on the irradiation dose, as shown in Fig. 7(a). The shape of the dose response curve is comparable to SrF_2:Er,Yb (Fig. 4(a)). The initial relative decay time reduction for 50 kGy amounts to 29% for SrF_2:Ho,Yb and 27% for SrF_2:Tm,Yb phosphor, similar to the 30% for SrF_2:Er,Yb.

For samples irradiated with 5 kGy and for unirradiated samples the luminescence decay times were repeatedly measured until 140 days after irradiation (Fig. 7(b)). Measurements on SrF_2:Tm,Yb suffer from significantly higher uncertainties compared to SrF_2:Ho,Yb despite the same processing of the powders and treatment of the samples. For Ho, Yb codoped SrF_2, we see all decay times lying within a range of 3 µs which corresponds to about 4% of the mean value measured after 5 kGy irradiation. This is, therefore, the upper estimation for the measured fading over 140 days, as no trend is observed in the time series. That is even lower than in SrF_2:Er,Yb, although with Er, a higher dose resolution was achieved.

Radiation-induced changes in doped SrF_2

After irradiation of the SrF_2:Er,Yb samples, we observed new reflections in their powder XRD (Fig. 8), likely from a newly formed secondary phase. The reference material $NaYF_4$:Er,Yb shows no additional reflections after the same irradiation dose (data not shown). Moreover, fluorescence spectroscopy
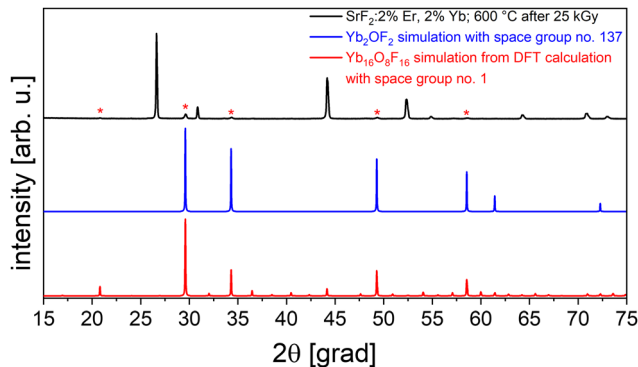

Fig. 8 X-ray diffraction pattern of SrF_2: 2%Er,2% Yb after irradiation (top, black; 10 MeV electron radiation, 25 kGy) with reflections observed only after irradiation marked with asterisks. Calculated X-ray diffraction pattern of the structure derived from Sm_2OF_2 (blue), and from the DFT calculation after refinement (red, structure 1 derived from Mn_2OF_2).

measurements were performed on irradiated and non-irradiated powders, using an excitation wavelength of 365 nm and fluorescence detection in the visible range (Fig. 9). We observe an emission band between 400 nm and 450 nm (peak at 421 nm) and another one between 460 nm and 700 nm (peak at about 560 nm) for irradiated powders. Both emissions are only barely observed in unirradiated powders. Based on literature data,[24–26] we assign the peak at 421 nm to the regular emission $4f^{13} 5d \rightarrow 4f^{14}$ of Yb^{2+}. The literature data on the spectral position of this emission ranges from 412 nm[25] to 447 nm.[26] Differences can be attributed to the varying crystal field in different host lattices and its effect on the excited d-levels of Yb^{2+}. The second, broader emission band can be attributed to the inter valence charge transfer (IVCT) emission of Yb in SrF_2 which is described as the transition $Yb^{2+} [^2F_{5/2} E_g (5d)-^2A_{1u}] + Yb^{3+} -> Yb^{3+} [^2F_{7/2}-G_{7u}] + Yb^{2+} [4f^{14}-A_{1g}]$ at 521 nm.[24]

Apparently, electron irradiation of SrF_2:Er,Yb led to the reduction of Yb^{3+} to Yb^{2+} (as observed *e.g.* upon irradiation in Yb^{3+}-doped CaF_2[27]) and to the formation of a secondary crystalline phase.

Returning to the XRD again, the new reflections were all weak in intensity compared to doped SrF_2 but fit well to a cubic indexation with a volume per formula unit V/FU = 150 Å³.
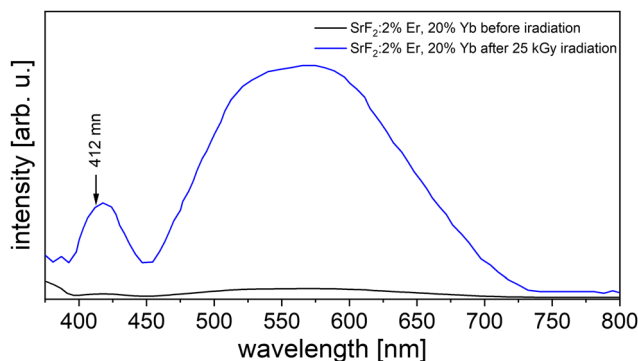

Fig. 9 Fluorescence emissions spectra of 25 kGy irradiated (blue) and non-irradiated (black) SrF_2 with 2 mol% Er and 20 mol% Yb.

This journal is © The Royal Society of Chemistry 2022

J. Mater. Chem. C, 2022, **10**, 11579–11587 | **11583**

The reflections did not fit to known, plausible compounds of both Yb^{2+} or Yb^{3+}; in fact, YbO is smaller (V/FU = 103 Å^3)[28] while YbF_2 is larger (V/FU = 175 Å^3)[29] than the observed phase. The formation of an oxide fluoride with an intermediate volume is thinkable: the powders were irradiated under air, and Yb^{3+} forms the well-described YbOF[30] (that however does not fit). Using the OQMD (Open Quantum Materials Database),[31] we identified the structure of Sm_2OF_2 as a possible starting point for the radiation-induced phase in SrF_2:Er,Yb. After substituting Sm by Yb and refining the cell parameters, the calculated reflections of the hypothetical structure principally match the measured ones (see Fig. 8, blue graph). However, there is a weak reflection in the measurements at 21° that cannot be explained by this structural model.

At this point, we turned to *ab initio* simulations in our search for a structural understanding of the secondary phase formed under irradiation. Thus, we performed DFT-based harmonic phonon computations and obtained additional structural models for Yb_2OF_2 from the Materials Project.[32] The computation of phonon band structures allows to confirm the dynamic stability of a material and thus to estimate the plausibility of a structural model. Further computational details can be found in the Method section and the ESI.†

As the result, among five candidates we found a dynamically stable structure based on a Mn_2OF_2 prediction[32] that is also the energetically most stable (see Table S1 in ESI† for further details). VESTA[33] was used to visualize its crystal structure, as seen in Fig. 10. With this structure predicted from DFT, after refinement of the cell parameters, we obtain a very good agreement of calculated and measured reflections in the XRD pattern (Fig. 8, red curve). The proposed compound is triclinic with a cell volume of 598 Å^3 and 4 formula units per elementary cell. This is in close agreement with our earlier assumption that the normalized cell volume should be approximately 150 Å^3.

The combined interpretation of our measurements and simulations indicates that Yb^{3+} in SrF_2:Er,Yb is partially reduced by the electron beam, and (some) Yb^{2+} segregates to form a secondary phase. Likely, this involves a reaction with air to form Yb_2OF_2, isostructural to Mn_2OF_2, but this must be verified independently. In any case, the formation of a secondary phase seems to be responsible for the irreversible change in the decay time of SrF_2:Er,Yb (at least in the time frame of our study).
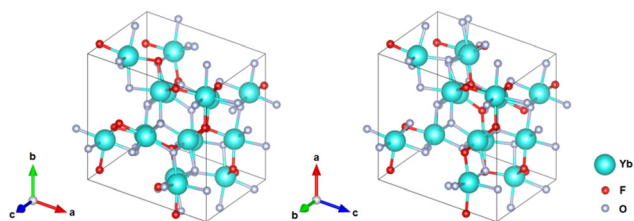

Fig. 10 Most stable predicted structure for Yb_2OF_2 by the DFT calculations as visualized by VESTA.[33]

Experimental

Synthetic procedures

To synthesize different rare-earth doped SrF_2 powders, we followed the procedure from ref. 16. $Sr(NO_3)_2$ (Sigma-Aldrich, purity 99.98%), $Yb(NO_3)_3 \cdot 6H_2O$ (Sigma-Aldrich, purity 99.99%), an additional rare earth nitrate (all Sigma Aldrich purity 99.99%), and distilled water were used as starting materials without additional purification. The additional RE nitrate used was either $Er(NO_3)_3 \cdot 5H_2O$, $Ho(NO_3)_3 \cdot 5H_2O$ or $Tm(NO_3)_3 \cdot 5H_2O$. As precipitant, ammonium fluoride (MerckMillipore) was used. Aqueous solutions of nitrates (0.08 M) and a 0.16 M aqueous solution of ammonium fluoride (for 2% Yb 7% molar excess[10,16] and 3-fold excess for 20% Yb[19]) were prepared by mixing the aforementioned salts with deionized water. The ammonium fluoride solution was added dropwise to the solution of nitrates under vigorous stirring: the formed suspension was stirred for 3 hours and then washed with a dilute solution of NH_4F. Finally, the suspension was centrifuged at 5000 rpm, and the precipitate recovered and dried at 40 °C for 6 h. Calcination of the material was carried out at 800 °C (SrF_2:Er,Yb) and 600 °C (SrF_2:Ho,Yb; SrF_2:Tm,Yb) in air.

Optical methods

Thin phosphor film preparation. Thin layers containing the phosphor particles were prepared as follows: phosphor powder was pestled in a mortar to break down agglomerations. Then, a varnish was prepared by first suspending the particles in ethanol and acetone, then adding a dispersing agent (Tego Dispers 755 W) and finally polyvinyl acetate (molecular weight approx. 500 000 g mol^{-1}) as binding agent and film former. Several single drops of a few μl were pipetted onto glass substrates to obtain phosphor particles immobilized in a thin layer that can be penetrated by the 200 keV electron beam radiation. The layer thickness was 50 to 60 μm.

Irradiation. The thin film samples were irradiated in an EBLab 200 electron irradiator (Comet) using 200 kV acceleration voltage. The air gap between the exit window of the electron radiation and the sample surface was 10 mm. Doses of 5 kGy up to 50 kGy were applied to the samples. Powder samples for X-ray diffractometry were irradiated at 10 MeV in a Van de Graaff electron beam accelerator.

Luminescence decay time measurements: to measure luminescence decay curves, excitation of the phosphor samples was carried out with a 1 ms light pulse from a 980 nm laser diode (max. 80 mW, Roithner) and the temporal luminescence decay was recorded by a silicon photodiode (Osram SFH2200). Note that no spectral filter is built into the detection path and, therefore, both visible UC and near-IR fluorescence emission contribute to the signal. Ten consecutive curves were averaged and then exponentially fitted to obtain the decay time. To assess the fading behavior after electron irradiation, we repeatedly measured the decay times of the samples in a time lapse of up to 140 days, starting with the first measurement immediately after irradiation. These first measurements were used to obtain the dose response curve. Between the measurements, the samples

were stored in the dark at room temperature. The luminescence spectra were acquired by the excitation of a pressed powder sample with 980 nm continuous wave laser light and recording the emitted light using a spectrometer (Horiba iHR 550).

Fluorescence spectroscopy. Yb^{2+}-fluorescence in SrF_2 was measured with a fluorescence spectrometer (Edinburgh Inst. FLS 920). Emission spectra were recorded upon the excitation at 365 nm.[25]

X-Ray and electron microscopy method

X-Ray. The X-ray phase analyses were carried out using a Bragg–Brentano X-ray diffractometer Bruker D8 Advance in reflection geometry. Powder samples were installed in the rotating sample holder. Monochromatic Cu Kα radiation (λ = 0.15406 nm) with an excitation voltage of 40 kV and a current of 30 mA were used. The radiation was diffracted on the sample and registered by an energy-dispersive 1D detector (LYNXEYE XE). There are constructive and destructive interferences depending on the measured angle (0.02 2θ-steps). The recorded reflections in the measuring range $5 \leq 2\theta \leq 90$ were assigned and evaluated by comparison with databases of known structures in the form of comparison line diagrams (EVA evaluation software DIFFRAC.EVA version 3.0 from Bruker).

Electron microscopy. Powder particles were carefully deposited onto a conductive tape, and then coated with an approx. 10 nm thick carbon layer. In the field emission electron microscope (Zeiss Extremist 55 plus), the particle morphology was well recognizable by means of secondary electrons (SEM, topography contrast). The images were acquired with 10.00 kV acceleration voltage and a working distance of WD = 6.8 mm, using an InLens detector.

DFT computations. We created structural models for Yb_2OF_2 based on chemically similar structures from the OQMD and the Materials Project. Some of the structures were chosen based on similar ionic radii of the cations, others were created with the algorithm described by Hautier et al.[13] We optimized the structures with periodic DFT in VASP[34–37] with strict convergence criteria. After the optimization, we derived five different structures (see ESI,† Fig. S1) using the PBE functional for all calculations.[38] All k-point settings were converged and can be found in the raw data ESI.† For electronic and structural optimization, a criterion of $\Delta E < 10^{-7}$ eV and $\Delta E < 10^{-5}$ eV per cell was used, respectively. Once the optimized structures were obtained, the harmonic interatomic force constants were computed using the finite displacement method as implemented in Phonopy,[39] with a displacement of 0.01 Å and with the help of supercell of the optimized cell (with cell parameters as close as possible to 20 Å or larger in each direction to ensure convergence). The forces for this evaluation were computed at the Γ-point. The depicted band structures have not been corrected with the non-analytical term correction around the Gamma point as this is not decisive for predicting dynamical stability. Robocrystallographer[40] and ChemEnv[41] were used to help describing and understanding the newly predicted structures. More information on the other structures can be found in the ESI.†

Conclusion

Considering the importance of the reliability of a dosimeter signal after irradiation, in this work, a series of SrF_2-based phosphors was synthesized aiming for their application as low-fading dosimeter materials. To this end, sub-micron SrF_2 powders codoped with Yb^{3+} sensitizer and different activator ions (Er^{3+}, Ho^{3+} and Tm^{3+}) were synthesized by the precipitation from aqueous solutions and calcination, and their crystal structures were characterized. Encouragingly, the SrF_2 materials show a dose-dependent reduction of their luminescence decay time and – most important – very low fading of the luminescence decay time compared to the previously studied $NaYF_4$:Yb^{3+},Er^{3+}. Upon irradiation, we observed the formation of Yb^{2+} from spectroscopy and a secondary phase from XRD. Together with DFT calculations, we suggest that this phase could be Yb_2OF_2 and predict a stable structure of it. The formation of this secondary phase could be the reason for the irreversible change in decay time, i.e. low fading. Therefore, future investigations will focus on a detailed multifactorial study of parameters like dose, dose rate, radiation energy and irradiation modality to further evaluate this promising dosimeter material.

Conflicts of interest

There are no conflicts to declare.

Acknowledgements

References

1 H. Aisala, H. Nygren, T. Seppänen-Laakso, R.-L. Heiniö, M. Kießling, K. Aganovic, A. Waser, H. Kotilainen and A. Ritala, Comparison of low energy and high energy electron beam treatments on sensory and chemical properties of seeds, *Food Res. Int.*, 2021, **148**, 110575.

2 Y. Zhang, N. Huber, R. Moeller, J. Stülke, B. Dubovcova, G. Akepsimaidis, N. Meneses, D. Drissner and A. Mathys, Role of DNA repair in Bacillus subtilis spore resistance to high energy and low energy electron beam treatments, *Food Microbiol.*, 2020, **87**, 103353.

3 J. Fertey, M. Thoma, J. Beckmann, L. Bayer, J. Finkensieper, S. Reißhauer, B. S. Berneck, L. Issmail, J. Schönfelder, J. P. Casado, A. Poremba, F.-H. Rögner, B. Standfest,

This journal is © The Royal Society of Chemistry 2022

J. Mater. Chem. C, 2022, **10**, 11579–11587 | 11585

G. R. Makert, L. Walcher, A.-K. Kistenmacher, S. Fricke, T. Grunwald and S. Ulbert, Automated application of low energy electron irradiation enables inactivation of pathogen- and cell-containing liquids in biomedical research and production facilities, *Sci. Rep.*, 2020, **10**, 12786.

4 M. R. Farukhi and C. F. Swinehart, Barium fluoride as a gamma ray and charged particle detector, *IEEE Trans. Nucl. Sci.*, 1971, **18**, 200–204.

5 G. Ban and H. N. Hersh, Degradation of some IR upconverting phosphors by ionizing radiation, *J. Electron. Mater.*, 1972, 320–332.

6 H. N. Hersh and G. Ban, X-ray—induced variation of time constant of Yb^{3+} sensitizer, *Appl. Phys. Lett.*, 1972, **20**, 101–102.

7 M. Reitzig, M. Winkler, T. Härtling, O. Röder and J. L. Opitz, Evaluation of low energy electron beam dose application by means of a portable optical device, *Opt. Eng.*, 2014, **53**, 1–3.

8 M. Reitzig, R. J. Goodband, C. Schuster and T. Härtling, Optical electron beam dosimetry with ceramic phosphors as passive sensor material for broad dose ranges, *Tech. Mess.*, 2016, **83**, 174.

9 C. Schuster, F. Kuntz, D. Cloetta, M. Zeller, J. Katzmann, A. Strasser, T. Härtling and M. Lavalle, Depth dose curve and surface dose measurement with a μm thin dosimetric layer, *Radiat. Phys. Chem.*, 2022, **193**, 109881.

10 G. Wang, Q. Peng and Y. Li, Upconversion luminescence of monodisperse $CaF_2:Yb^{3+}/Er^{3+}$ nanocrystals, *J. Am. Chem. Soc.*, 2009, **131**, 14200–14201.

11 Z. Wang, J. Ha, Y. H. Kim, W. B. Im, J. McKittrick and S. P. Ong, Mining unexplored chemistries for phosphors for high-color-quality white-light-emitting diodes, *Joule*, 2018, **2**, 914–926.

12 J. George and G. Hautier, Chemist versus machine: Traditional knowledge *versus* machine learning techniques, *Trends Chem.*, 2021, **3**, 86–95.

13 G. Hautier, C. Fischer, V. Ehrlacher, A. Jain and G. Ceder, Data mined ionic substitutions for the discovery of new compounds, *Inorg. Chem.*, 2011, **50**, 656–663.

14 P. P. Fedorov, A. A. Alexandrov, V. V. Voronov, M. N. Mayakova, A. E. Baranchikov and V. K. Ivanov, Low-temperature phase formation in the SrF_2–LaF_3 system, *J. Am. Ceram. Soc.*, 2021, **104**, 2836–2848.

15 W. Li, B. Mei, J. Song and Z. Wang, Fabrication and optical property of highly transparent SrF_2 ceramic, *Mater. Lett.*, 2015, **159**, 210–212.

16 S. Kuznetsov, Y. Ermakova, V. Voronov, P. Fedorov, D. Busko, I. A. Howard, B. S. Richards and A. Turshatov, Up-conversion quantum yields of $SrF_2:Yb^{3+},Er^{3+}$ sub-micron particles prepared by precipitation from aqueous solution, *J. Mater. Chem. C*, 2018, **6**, 598–604.

17 S. V. Kuznetsov and P. P. Fedorov, Morphological stability of solid-liquid interface during melt crystallization of $M_{1-x}R_xF_{2+x}$ solid solutions, *Inorg. Mater.*, 2008, **44**, 1434–1458.

18 A. A. Lyapin, P. A. Ryabochkina, S. V. Gushchin, S. V. Kuznetsov, M. V. Chernov, V. Y. Proydakova, V. V. Voronov and P. P. Fedorov, Upconversion luminescence of fluoride phosphors $SrF_2:Er,Yb$ under laser excitation at 1.5 μm, *Opt. Spectrosc.*, 2018, **125**, 537–542.

19 D. Przybylska, A. Ekner-Grzyb, B. F. Grześkowiak and T. Grzyb, Upconverting SrF_2 nanoparticles doped with Yb^{3+}/Ho^{3+}, Yb^{3+}/Er^{3+} and Yb^{3+}/Tm^{3+} ions – optimisation of synthesis method, structural, spectroscopic and cytotoxicity studies, *Sci. Rep.*, 2019, **9**, 8669.

20 Y. Gao, B. Mei, W. Li, Z. Zhou and Z. Liu, Effect of Yb^{3+} concentration on microstructure and optical properties of Yb: SrF_2 transparent ceramics, *Opt. Mater.*, 2020, **105**, 109869.

21 M. S. Bhadane, K. H. Gavhane, V. S. Ghemud, S. S. Dahiwale, P. S. Patil, A. Kshirsagar and S. D. Dhole, A post annealing effect on SrF_2 nano particles: Structural, morphological, functional and dosimetric properties, *J. Alloys Compd.*, 2020, **846**, 156343.

22 T. Kojima, L. Chen, Y. Haruyama, H. Tachibana and R. Tanaka, Fading characteristics of an alanine-polystyrene dosimeter, *Appl. Radiat. Isot.*, 1992, **43**, 863–867.

23 I. Nicoara, L. Lighezan, M. Enculescu and I. Enculescu, Optical spectroscopy of Yb^{2+} ions in YbF_3-doped CaF_2 crystals, *J. Cryst. Growth*, 2008, **310**, 2026–2032.

24 Z. Barandiarán and L. Seijo, Intervalence charge transfer luminescence: Interplay between anomalous and 5d–4f emissions in Yb-doped fluorite-type crystals, *J. Chem. Phys.*, 2014, **141**, 234704.

25 M. Suta, W. Urland, C. Daul and C. Wickleder, Photoluminescence properties of Yb(2+) ions doped in the perovskites $CsCaX_3$ and $CsSrX_3$ (X = Cl, Br, and I) – a comparative study, *Phys. Chem. Chem. Phys.*, 2016, **18**, 13196–13208.

26 M. Suta, T. Senden, J. Olchowka, M. Adlung, A. Meijerink and C. Wickleder, Decay times of the spin-forbidden and spin-enabled transitions of Yb^{2+} doped in $CsCaX_3$ and $CsSrX_3$ (X = Cl, Br, I), *Phys. Chem. Chem. Phys.*, 2017, **19**, 7188–7194.

27 D. S. McClure and Z. Kiss, Survey of the spectra of the divalent rare-earth ions in cubic crystals, *J. Chem. Phys.*, 1963, **39**, 3251–3257.

28 O. Reckeweg and F. J. DiSalvo, Single-crystal structure refinement of YbF_2 with a remark about YbH_2, *Z. Naturforsch., B: J. Chem. Sci.*, 2017, **72**, 995–998.

29 A. Goto, Y. Ohta and M. Kitayama, Solid-state synthesis of metastable ytterbium(II) oxide, *J. Mater. Sci. Chem. Eng.*, 2018, **6**, 85.

30 T. Wen, Y. Zhou, Y. Guo, C. Zhao, B. Yang and Y. Wang, Color-tunable and single-band red upconversion luminescence from rare-earth doped Vernier phase ytterbium oxyfluoride nanoparticles, *J. Mater. Chem. C*, 2016, **4**, 684–690.

31 The Open Quantum Materials Database, https://oqmd.org/.

32 The Materials Project database, https://materialsproject.org/.

33 K. Momma and F. Izumi, VESTA 3 for three-dimensional visualization of crystal, volumetric and morphology data, *J. Appl. Crystallogr.*, 2011, **44**, 1272–1276.

34 G. Kresse, J. Furthmüller and J. Hafner, Theory of the crystal structures of selenium and tellurium: The effect of generalized-gradient corrections to the local-density approximation, *Phys. Rev. B: Condens. Matter Mater. Phys.*, 1994, **50**, 13181.

11586 | *J. Mater. Chem. C*, 2022, **10**, 11579–11587

This journal is © The Royal Society of Chemistry 2022

35 G. Kresse and J. Hafner, *Ab initio* molecular dynamics for liquid metals, *Phys. Rev. B: Condens. Matter Mater. Phys.*, 1993, **47**, 558–561.

36 G. Kresse and J. Furthmüller, Efficiency of *ab initio* total energy calculations for metals and semiconductors using a plane-wave basis set, *Comput. Mater. Sci.*, 1996, **6**, 15–50.

37 G. Kresse and J. Furthmüller, Efficient iterative schemes for *ab initio* total-energy calculations using a plane-wave basis set, *Phys. Rev. B: Condens. Matter Mater. Phys.*, 1996, **54**, 11169.

38 J. P. Perdew, K. Burke and M. Ernzerhof, Generalized gradient approximation made simple, *Phys. Rev. Lett.*, 1996, **77**, 3865.

39 A. Togo and I. Tanaka, First principles phonon calculations in materials science, *Scr. Mater.*, 2015, **108**, 1–5.

40 A. M. Ganose and A. Jain, Robocrystallographer: Automated crystal structure text descriptions and analysis, *MRS Commun.*, 2019, **9**, 874–881.

41 D. Waroquiers, J. George, M. Horton, S. Schenk, K. A. Persson, G.-M. Rignanese, X. Gonze and G. Hautier, ChemEnv: A fast and robust coordination environment identification tool, *Acta Crystallogr., Sect. B: Struct. Sci., Cryst. Eng. Mater.*, 2020, **76**, 683–695.

This journal is © The Royal Society of Chemistry 2022

J. Mater. Chem. C, 2022, **10**, 11579–11587 | 11587